Mode-degeneracy lifting in exceptional points of a coupled spaser-dielectric waveguide system

Anton V. Hlushchenko,* Vitalii I. Shcherbinin, and Oksana L. Andrieieva
National Science Center "Kharkiv Institute of Physics and Technology" of National Academy of Sciences of Ukraine, 1 Akademicheskaya St., Kharkiv 61108, Ukraine

Viktor I. Tkachenko
National Science Center "Kharkiv Institute of Physics and Technology" of National Academy of Sciences of Ukraine, 1 Akademicheskaya St., Kharkiv 61108, Ukraine and Education and Research Institute of Computer Physics and Energy, V. N. Karazin Kharkiv National University, 4, Svobody Sq., Kharkiv 61022, Ukraine

Vladimir R. Tuz†
State Key Laboratory of Integrated Optoelectronics, College of Electronic Science and Engineering, International Center of Future Science, Jilin University, 2699 Qianjin St., Changchun 130012, China and School of Radiophysics, Biomedical Electronics and Computer Systems, V. N. Karazin Kharkiv National University, 4, Svobody Sq., Kharkiv 61022, Ukraine

(Received 30 May 2023; accepted 22 November 2023; published 19 December 2023)

One of the main requirements for advanced optical systems is controllability, which can be greatly improved by introducing gain elements into a guiding system. In this study, we consider a coupled photonic-plasmonic system composed of a dielectric waveguide and a three-layer (dielectric-metal-dielectric) waveguide spaser with loss and gain. Conditions of mode degeneracy in this system are revealed. A classification of waveguide and surface plasmon modes is used to find parameters of the formation of exceptional points (EPs) of the coupled system with loss and gain. It is shown that at these points the lifting of the mode degeneracy occurs. In addition, the response of the coupled system to illumination is investigated for incident Gaussian beams of two orthogonal polarizations. It is demonstrated that the control of the incident beam polarization makes it possible to excite different modes. The revealed operation conditions of the optical system with two-stage control (control of the EP parameters plus control of wave polarization) can widen the application range of coupled spaser-dielectric waveguide systems.

DOI: 10.1103/PhysRevA.108.063513

I. INTRODUCTION

One of the main challenges of photonics and plasmonics is the development of on-chip optical devices that provide better control over light at the nanoscale [1,2]. Dynamic control of a light wave can be achieved through the loss-gain distribution, and this is currently the subject of the rapidly developing field of non-Hermitian photonics [3]. The combination of loss and gain constituents within one system leads to the emergence of new optical functionalities such as parity-time ($\mathcal{PT}$) symmetries [4–7], exceptional points (EPs) [7,8], and loss compensation in waveguide systems [9], nanoparticles and their clusters [9–11], and metamaterials [12–14]. In addition to optics and photonics, studies of the gain-loss systems have culminated in discoveries in other fields of physics such as microwave techniques [15], electronics [16], optomechanics [17], and acoustics [18,19].

In optical systems, $\mathcal{PT}$-symmetry threshold and exceptional points [4,7] can also be supplemented by polarization degeneration of modes. This degeneracy is intrinsic to modes with a nonzero azimuthal index in circular waveguides [20] and resonators [21], and is related to field configuration and geometry of the system. Moreover, if the system is operated in the multimode conditions, a dispersion between several modes may occur (intermodal coupling) arising from the various modal propagation constants inside a multimode structure. It results in the pulse broadening as it is propagated inside the system [22] as well as causes mode-instability problems [23]. Therefore, controlling the conditions of the mode degeneracy and intermodal coupling makes it possible to reduce the manifestation of these shortcomings. However, the lifting of degeneracy when working on hybrid modes makes it possible to increase the density of transmitted information along the waveguide channel [24]. Separation of hybrid modes is usually carried out by introducing a spatial asymmetry or by considering the dispersion heterogeneity of the medium [25–31].

Optical structures can be divided into two major groups: metallic or semiconductor systems that support surface-plasmon modes and dielectric systems with modes localized inside the dielectric volume. Recently, hybrid systems, which consist of both metal and dielectric constituents,

*glushchenko.ant@gmail.com
†tvr@jlu.edu.cn

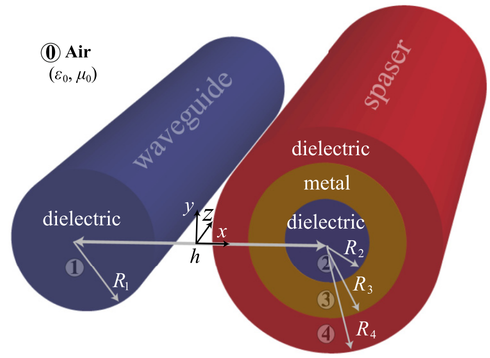

FIG. 1. Schematic illustration and geometric parameters of a spaser-dielectric waveguide system.

have attracted considerable interest [32,33]. Such photonic-plasmonic systems can take advantage of low losses of the dielectric materials and strong localization of the excited electromagnetic field inside metals at the nanoscale. This makes metal-dielectric structures very useful in many applications, including photonic components in sensing [34–36], surface-enhanced Raman spectroscopy [37,38], absorption and fluorescence [39–42], and nonlinear effect enhancement [43–45]. Hybrid metal-dielectric systems combined with active nanophotonics find use in laser applications. In this study, we are concerned with plasmonic nanolasers or spasers [46–49]. The widely used spaser structure consists of a dielectric core coated by a metal nanoshell and embedded into a monolayer of nanocrystalline quantum dots (gain) material [47,50].

Therefore, in this paper, we study a coupled system of a dielectric waveguide and a three-layer (dielectric-metal-dielectric) waveguide spaser. The operation principle of the system under consideration is based on the exceptional points existing in the dispersion characteristics of the waveguide modes of the dielectric waveguide and the surface-plasmon modes of the spaser. It is shown that the presence of exceptional points results in the lifting of the mode degeneracy in the system where the transition between the degenerate and non-degenerate states appears directly at these exceptional points. The observed features can be used to improve the ability to control nanolaser systems, by tuning both the exceptional point parameters and mode polarization. Our results can be considered as a development of the idea experimentally demonstrated in Ref. [4], taking into account that the problem is solved in a multimode configuration for the waveguide structure composed of photonic and plasmonic subsystems.

II. MODE DEGENERACY

In what follows, we consider a coupled system of a dielectric waveguide (photonic subsystem) and a spaser (plasmonic subsystem), which occupy regions 1 and 2 to 4, respectively, and are surrounded by air 0 as shown in Fig. 1. The waveguide has a form of an all-dielectric cylinder with radius R_1 and is coupled to a three-layer waveguide spaser, which is made from dielectric core 2 (with radius R_2) coated by metal shell 3 (with thickness $|R_3 - R_2|$) and surrounded by a layer of amplifying dielectric 4 (with thickness $|R_4 - R_3|$). The dielectric material of the waveguide and spaser is quartz ($\varepsilon'_{r1} = \varepsilon'_{r2} = \varepsilon'_{r4} = 4$). The dispersion properties of metal shell 3 are described by the Drude model (see Appendix A). The wave factor is chosen as $\exp[i(\omega t - k_z z)]$. Therefore, lossy and amplifying dielectric materials with relative complex permittivity $\varepsilon_{rj} = \varepsilon'_{rj} - i\varepsilon''_{rj}$ are characterized by $\varepsilon''_{r1,r2} > 0$ and $\varepsilon''_{r4} < 0$, respectively. Optical amplification in a quartz-based material can be implemented, for example, using methods for the synthesis of highly luminescent silica nanostructures [51,52].

In this study, we use a multimode analytical approach developed earlier [53,54] for the eigenmode analysis of coupled guiding systems (see Appendix B). Previously [54], a good numerical convergence and high accuracy of this approach were confirmed by comparison with simulation results obtained in the full-wave electromagnetic solver (COMSOL MULTIPHYSICS). Here, such a comparison is omitted for the sake of simplicity.

We begin with the classification of coupled modes supported by the dielectric waveguide and spaser. The modes of dielectric cylinder 1 can be classified as the axially symmetric TM_{0m} and TE_{0m} and asymmetric (hybrid) HE_{nm} and EH_{nm} modes [20,54]. For the waveguide spaser, we restrict our attention to the surface plasmon modes, which are designated as $Pl_1 \ldots Pl_n$. Here, the azimuthal index n of the mode increases from low- to high-frequency modes. As the distance h between the dielectric waveguide and spaser approaches infinity and the mode coupling vanishes, these modes transform to the pure waveguide modes for dielectric cylinder 1 and the surface plasmon modes for spaser 2 to 4. We classify degenerate modes as x or y polarized depending on the polarization of the incident Gaussian beam used for the system excitation.

Without loss of generality, we can fix some parameters of the system under consideration. In particular, the dimensions of the spaser remain unchanged below (see caption to Fig. 2). The properties of the spaser metal shell are chosen in accordance with tabular data and are close to those of silver (Ag) [55] (for details, see Appendix A).

The plots in Fig. 2(a) show frequencies of the low-order modes of the dielectric waveguide and spaser as functions of the radius of dielectric waveguide 1. The distance $h = 1600$ nm is chosen so that the mode interaction is very weak and can be neglected. Since modes of the spaser are independent of R_1, their frequencies remain constant. In the selected frequency range, the three lowest-order plasmon modes depicted in Fig. 2(a) are the axially symmetric mode Pl_1 and two frequency degenerate Pl_1^x and Pl_1^y modes, where their longitudinal electric field components $|E_z|$ are shown in Fig. 2(b). In addition to plasmon modes, there are the $HE_{11}^{x,y}$, TE_{01}, $HE_{21}^{x,y}$, and TM_{01} waveguide modes with axial field components ($|E_z|$ or $|H_z|$) depicted in Fig. 2(b). As in the case of plasmonic modes $Pl_2^{x,y}$, the hybrid $HE_{11}^{x,y}$ and $HE_{21}^{x,y}$ modes of the dielectric waveguide are degenerate.

III. EXCEPTIONAL POINTS MANIFESTATION

To achieve the mode degeneracy lifting, it is proposed to use the features of the exceptional points of the plasmon-dielectric interaction. For this purpose, we consider the crossings of the plasmon and waveguide modes, which can

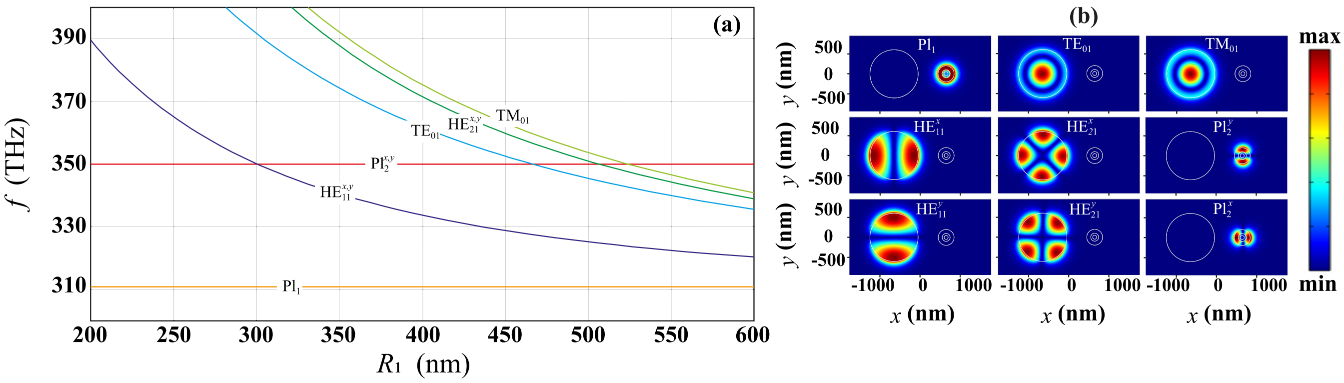

FIG. 2. (a) Dispersion curves of several low-order modes of a dielectric waveguide and a spaser ($k_z = 1.289\times10^7$ rad/m) and (b) magnitude of the dominant longitudinal field components plotted in the transversal cross section of the waveguide system when $R_1 = 600$ nm. The geometrical parameters of the spaser are $R_2 = 50$ nm, $R_3 = 2R_2$, and $R_4 = 4R_2$. The permittivity of the waveguide and dielectric layers of the spaser is $\varepsilon_1 = \varepsilon_2 = \varepsilon_4 = 12$. The Drude parameters for metallic layer of the spaser are $\varepsilon_\infty = 1.03$, $\omega_p = 1.3\times10^{16}$ rad/s and $\Gamma = 1.13\times10^{14}$ rad/s.

be seen in Fig. 2. Let the spaser be operated on the $\mathrm{Pl}_2^{x,y}$ modes at the frequency $f = 350$ THz. For completeness, it suffices to study the interaction of the hybrid $\mathrm{HE}_{11}^{x,y}$ and axially symmetric TM_{01} waveguide modes with the plasmonic $\mathrm{Pl}_2^{x,y}$ mode since other modes interact in much the same manner. Assume that the dielectric waveguide 1 and dielectric core 2 of the spaser have the same material losses $\varepsilon''_{r1} = \varepsilon''_{r2} = 0.001$. The value of gain ε''_4 in the outer layer of the spaser is chosen to compensate losses in the entire system.

The plots in Fig. 3(a) show the real and imaginary parts of the z component of the wave vector $\mathbf{k}$ of coupled Pl_2^x and TM_{01} modes as functions of the distance between the dielectric waveguide and spaser. For $R_1 = 522.31$ nm, there is an exceptional point of the plasmon-dielectric interaction at $h = h_{\mathrm{EP}} = 1117$ nm. At this point, a purely real value of k_z of the guiding system is achieved for $\varepsilon''_4 = -0.057$, which is sufficient to compensate for losses inherent in all system constituents. The obtained exceptional point serves as a transition between the system with ($h > h_{\mathrm{EP}}$) and without ($h < h_{\mathrm{EP}}$) the mode degeneracy. Thus, there are two origins of degeneracy in the system: (i) crossing of the modes of the waveguide and spaser at the exceptional point and (ii) convergence of the dispersion curve of the modes with nonzero azimuthal indices. Hence it follows that by maintaining the degeneracy of the "singular point" type [56], it is possible to lift the degeneracy of hybrid modes of the waveguide and spaser. To be more specific, the TM_{01} mode of waveguide 1 can be used to remove the degeneracy of plasmon Pl_2^x and Pl_2^y modes due to their coupling. The interaction between the TM_{01} mode and the x-polarized Pl_2^x mode is due to the specific spatial asymmetry of the given system with respect to the x axis.

The z component of the electric field $|E_z|$ is also presented for several points (1) to (4) depicted in Fig. 3(a). For points with the mode degeneracy ($h > h_{\mathrm{EP}}$), the electric field is mainly localized in either the dielectric waveguide or the spaser. For exceptional points and states with removed degeneracy ($h \leqslant h_{\mathrm{EP}}$), the field is hybridized and nonvanishing in all system components. Unlike $\mathcal{PT}$-symmetric gain-loss systems, asymmetric systems give a clue to the mode degeneration lifting of hybrid modes. Indeed, for a sufficiently large distance h and negligibly small mode interaction, we can always choose such a coordinate system for either the dielectric waveguide or the spaser that system (B7) is independent of the x and y polarization [$M(x) = M(-x)$ and $M(y) = M(-y)$]. In the case of strong coupling between modes of the system, its asymmetry results in $M(x) \neq M(-x)$ or $M(y) \neq M(-y)$.

Let us next consider the interaction of the hybrid waveguide $\mathrm{HE}_{11}^{x,y}$ modes and surface plasmon $\mathrm{Pl}_2^{x,y}$ modes, which undergo crossing at $R_1 = 299.28$ nm. The plots in Fig. 3(b) show the real and imaginary parts of k_z of the coupled modes. In this figure, two exceptional points are found for the HE_{11}^x-Pl_2^x and HE_{11}^y-Pl_2^y mode pairs. To fully compensate for losses at the exceptional points, the gain of the outer layer of the spaser is set equal to $\varepsilon''_4 = -0.057$. Due to the asymmetry of the system under consideration, exceptional points for modes with the x and y polarizations are observed for different distances $h = 937$ nm and $h = 896$ nm, respectively. For points (5) to (10) in Fig. 3(b), the magnitude of the longitudinal component of the electric field $|E_z|$ is plotted as color maps. These patterns suggest that for negligible interaction of both the x-polarized and y-polarized modes, the longitudinal component of the electric field is mainly presented in either the waveguide or spaser. By contrast, at exceptional points, the hybridized field is distributed throughout the entire guiding system.

In the above consideration, the mode interaction in the system was controlled by choosing an optimal distance between the waveguide and the spaser. Similar behavior of the system properties (as shown in Fig. 3) can be obtained by controlling values of the gain and loss. To do this, we can assume fixed distances h for the formation of exceptional points and then adjust the parameters of gain and loss.

IV. EXCITATION BY A GAUSSIAN BEAM

In this section, we investigate the effect of an external incident field on the excitation of plasmon-dielectric modes. We use a Gaussian beam as an external source of radiation, which makes it possible to focus the incident field in small volumes of space. This is important for better feedback

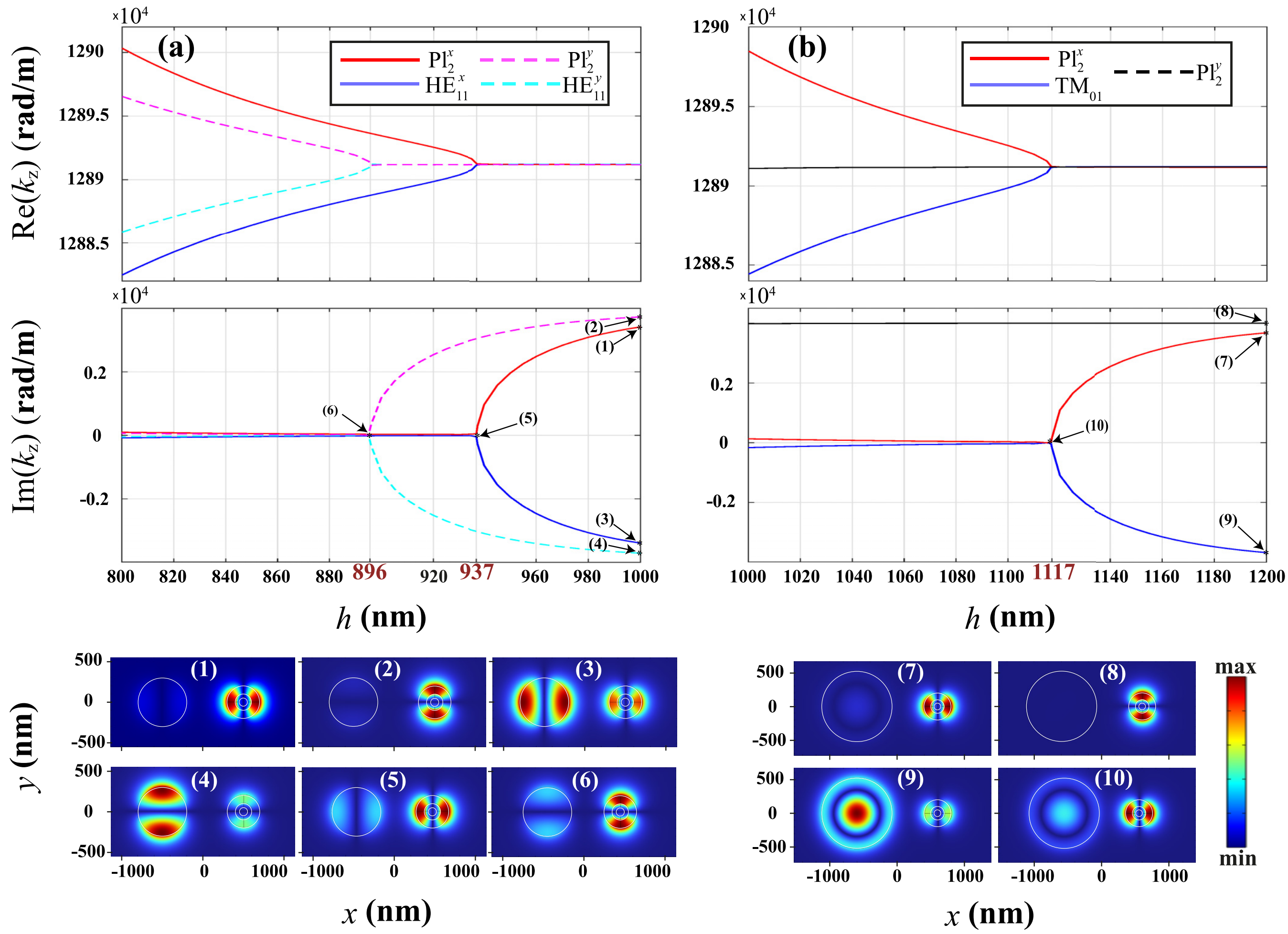

FIG. 3. The real (top panels) and imaginary (middle panels) parts of the eigenvalues k_z for the $Pl_2^{x,y}$ modes of the spaser and (a) the TM_{01} mode ($R_1 = 522.31$ nm) and (b) the $HE_{11}^{x,y}$ mode ($R_1 = 299.28$ nm) of the dielectric waveguide as functions of the distance h. The corresponding longitudinal components of the electric field $|E_z|$ for points (1)–(10) marked on the dispersion curves are shown separately on the bottom panels with color maps. The permittivity of the waveguide and dielectric layers of the spaser is $\varepsilon_1 = \varepsilon_2 = 12 - i0.001$. The permittivity of the gain layer of spaser is $\varepsilon_4'' = 12 + i0.057$.

control of integrated optical systems at the nanoscale [57,58]. The Gaussian beam equation in coordinates (η, ξ) is given in Appendix C. The presented Eqs. (C1) describe the Gaussian beam in the η direction, hence the x or y polarization of the field is defined as $\eta = x$, $\xi = y$ or $\eta = y$, $\xi = x$, respectively.

To analyze the excited modes of the considered spaser system of the volume V, we calculate the electric energy stored in the system. The integral of the electric energy in the volume V can be written as a sum of energies of each component of the system V_i ($i = 1 \dots 4$),

$$U_e = \sum_{i=1}^{4} \frac{\varepsilon_i}{2} \int_{V_i} |\mathbf{E}|^2 dV_i. \qquad (1)$$

Figure 4(a) corresponds to the excitation of the axially symmetric waveguide TM_{01} and spaser Pl_2^x modes by the x-polarized external Gaussian beam. These modes also form an exceptional point on the corresponding dispersion curves which are depicted on the bottom plane of the figure. In addition, for selected points (1) to (3), the longitudinal components of the electric field $|E_z|$ excited by the beam are collected in the form of color maps. We should note that the system has no response when exposed to the y-polarized external Gaussian beam. Therefore, the Pl_2^y mode is "dark" and is not excited by an external source.

Further, we are interested in the manifestation of the interaction of hybrid waveguide modes with plasmon ones. In particular, the excitation of the HE_{11}^x and Pl_2^x modes by the external x-polarized Gaussian beam are presented in Fig. 4(b) as a function of the frequency and distance h, whereas Fig. 4(c) shows the excitation of another pair of the HE_{11}^y and Pl_2^y modes by the y-polarized Gaussian beam. For points (4) to (9) depicted in this figure, the longitudinal components of the electric field $|E_z|$ are also shown. In addition, the contributions of modes to the electric energy are calculated for all found exceptional points (see Appendix D). The obtained results confirm that the excitation of modes with different polarizations can be provided by controlling the polarization of the external beam. However tuning the exceptional point conditions by changing the distance between the spaser and the waveguide leads to the possibility of controlling the mode

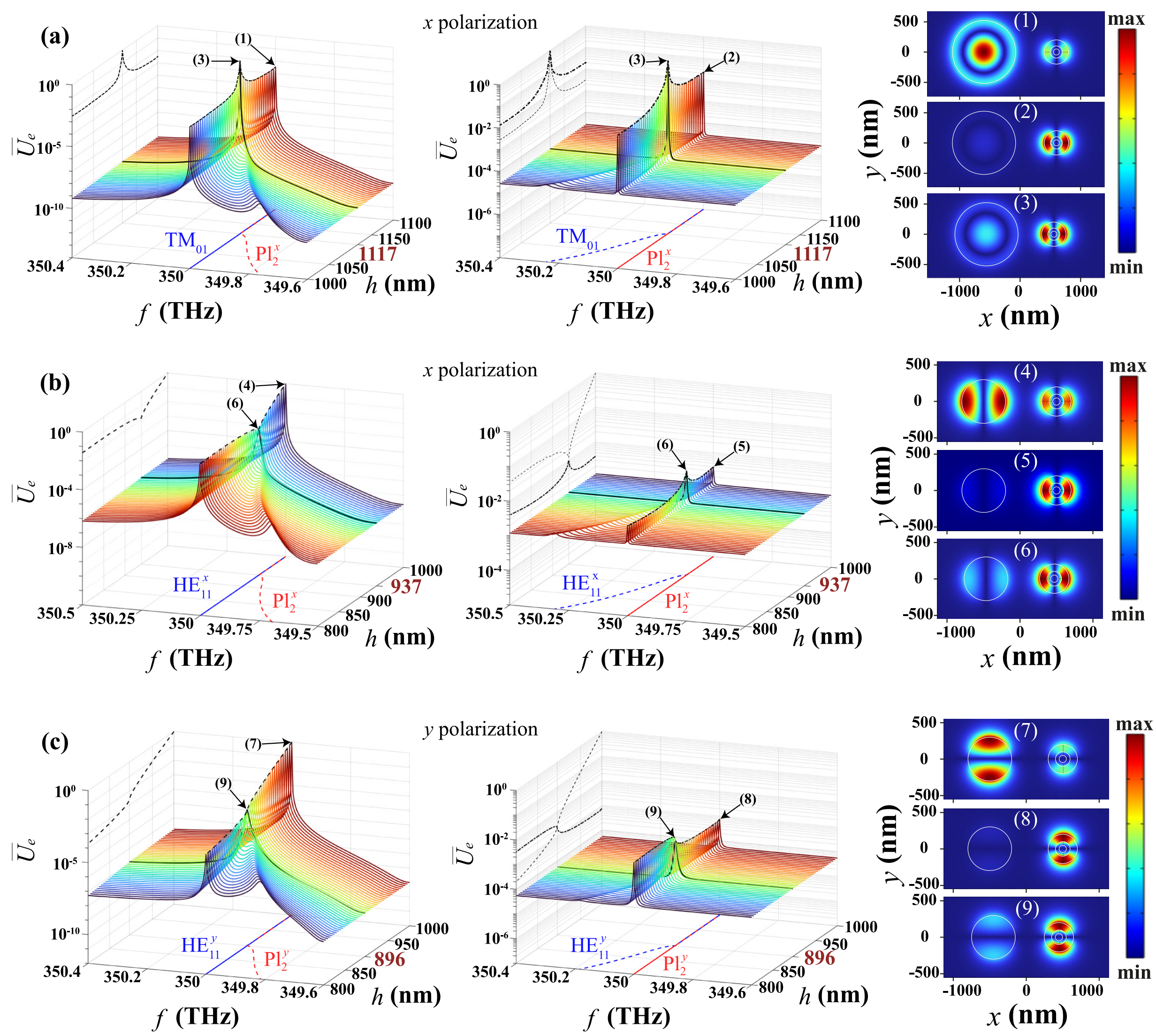

FIG. 4. Electric energy stored in the system $\bar{U}_e = U_e/\max(U_e)$ for (a) TM_{01} and PL_2^x, (b) HE_{11}^x and PL_2^x, and (c) HE_{11}^y and PL_2^y mode pairs as a function of the frequency f and the distance h between the waveguide and spaser in the case of the system irradiation by the x- and y-polarized Gaussian beam. The longitudinal components of the electric field $|E_z|$ are plotted at the corresponding points (1)–(9). The Gaussian beam parameters are $x_0 = -d/2$, $y_0 = 0$ for the waveguide modes, and $x_0 = d/2$, $y_0 = 0$ for the spaser modes. All parameters of the system are the same as listed in captions for Figs. 2 and 3.

degeneracy and their separation. Thus we present an optical system with a high degree of controllability, which significantly expands the scope of its implementation.

V. CONCLUSION

We applied a multimode approach to the analysis of the coupled photonic-plasmonic system of the dielectric waveguide and three-layer (dielectric-metal-dielectric) waveguide spaser. We studied the interaction between the waveguide modes of the dielectric cylinder and the surface-plasmon modes of the spaser, with particular emphasis on the hybrid waveguide or hybrid plasmon modes characterized by degeneracy. The exceptional points caused by coupling between the waveguide and plasmon modes were found. The coupling in the system can be tuned by changing the distance h between the waveguide and spaser. It was shown that the coupled system features the mode degeneracy, provided that h is greater than the value at the exceptional point. It was found that the exceptional point enables the mode degeneracy lifting and coupled modes of different polarizations exhibit distinct frequency change with further decrease in h.

Excitation of the x- and y-polarized modes was investigated in relation to the polarization of the incident Gaussian beam. Excitation of different types of modes was achieved by controlling the beam polarization and the shift h relative to the value at the exceptional point. Thus, the considered system shows the ability to control optical wave properties by tuning the exceptional point location and polarization of the incident wave. Such a two-stage control significantly expands the applications of this structure in hybrid photonic-plasmonic systems.

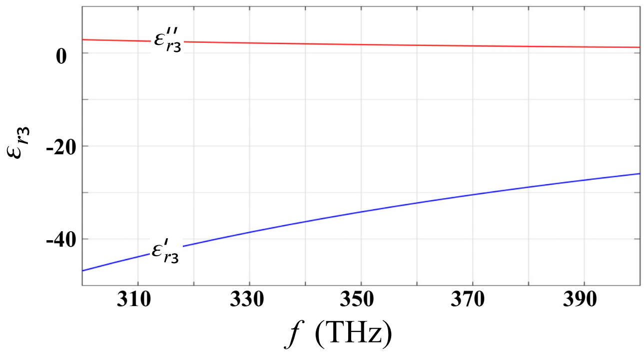

FIG. 5. The real ε'_{r3} and imaginary ε''_{r3} parts of the permittivity ε_{r3} as a function of the frequency f. The following parameter values are chosen: $\varepsilon_\infty = 1.03$, $\omega_p = 1.3\times10^{16}$ rad/s and $\Gamma = 1.13\times10^{14}$ rad/s.

ACKNOWLEDGMENTS

A.V. H. is supported by the grant of the National Academy of Sciences of Ukraine (NASU) to research laboratories and groups of young scientists of NASU for conducting research in priority areas of science and technology (Grant No. 0122U002145). V.R.T. is grateful for the hospitality and support from Jilin University, China.

APPENDIX A: DRUDE MODEL

The permittivity of metal shell 3 depends on the frequency ω and is described by the Drude model as

$$\varepsilon_3/\varepsilon_0 = \varepsilon_{r3}(\omega) = \varepsilon_\infty - \frac{\omega_p^2}{\omega^2 + i\Gamma\omega}, \tag{A1}$$

where the constant $\varepsilon_\infty > 1$ is the correction for high-frequency terms that are not explicitly modeled, ω_p is the plasma frequency, and Γ is the damping coefficient. Figure 5 shows the behavior of the frequency-dependent permittivity (A1), which is close to the tabular data from [55] for the permittivity of silver (Ag).

APPENDIX B: MULTIMODE APPROACH

To analyze the coupled spaser-waveguide system, we use a multimode analytical approach [53,54]. In this paper, we consider the coupling of a dielectric circular waveguide (region 1 in Fig. 1) with a three-layer (dielectric-metal-dielectric) waveguide spaser (regions 2 to 4 in Fig. 1). To solve the eigenvalue problem for this system, we consider two polar coordinate frames (r_1, ϕ_1) and (r_2, ϕ_2) whose centers coincide with the centers of dielectric waveguide 1 and spaser 2 to 4, respectively. In terms of these coordinates, we write the E_z and H_z components of electromagnetic fields for all regions 0 and 1 to 4 as sums of spatial azimuthal harmonics. First, in region 1, we have

$$E_z^1 = \sum_{n=-N}^{N} A_n^1 J_n(k_{p,1} r_1) e^{in\phi_1},$$

$$H_z^1 = \sum_{n=-N}^{N} B_n^1 J_n(k_{p,1} r_1) e^{in\phi_1}. \tag{B1}$$

In all regions 2 to 4 of the spaser, we use coordinates (r_2, ϕ_2) and can write

$$E_z^2 = \sum_{n=-N}^{N} A_n^2 J_n(k_{p,2} r_2) e^{in\phi_2},$$

$$H_z^2 = \sum_{n=-N}^{N} B_n^2 J_n(k_{p,2} r_2) e^{in\phi_2}, \tag{B2}$$

for dielectric core 2 with $r_2 \leqslant R_2$,

$$E_z^3 = \sum_{n=-N}^{N} A_n^3 J_n(k_{p,3} r_2) e^{in\phi_2} + \sum_{n=-N}^{N} C_n^3 Y_n(k_{p,3} r_2) e^{in\phi_2},$$

$$H_z^3 = \sum_{n=-N}^{N} B_n^3 J_n(k_{p,3} r_2) e^{in\phi_2} + \sum_{n=-N}^{N} D_n^3 Y_n(k_{p,3} r_2) e^{in\phi_2}, \tag{B3}$$

for metal shell 3 with $R_2 < r_2 \leqslant R_3$, and

$$E_z^4 = \sum_{n=-N}^{N} A_n^4 J_n(k_{p,4} r_2) e^{in\phi_2} + \sum_{n=-N}^{N} C_n^4 Y_n(k_{p,4} r_2) e^{in\phi_2},$$

$$H_z^4 = \sum_{n=-N}^{N} B_n^4 J_n(k_{p,4} r_2) e^{in\phi_2} + \sum_{n=-N}^{N} D_n^4 Y_n(k_{p,4} r_2) e^{in\phi_2}, \tag{B4}$$

for the layer of amplifying dielectric 4 with $R_3 < r_2 \leqslant R_4$.

In region 0, the field is expressed in terms of coordinates of both local coordinate frames as

$$E_z^0 = \sum_{n=-N}^{N} C_n^1 H_n^{(1,2)}(k_{p,0} r_1) e^{in\phi_1} + \sum_{n=-N}^{N} C_n^2 H_n^{(1,2)}(k_{p,0} r_2) e^{in\phi_2},$$

$$H_z^0 = \sum_{n=-N}^{N} D_n^1 H_n^{(1,2)}(k_{p,0} r_1) e^{in\phi_1} + \sum_{n=-N}^{N} D_n^2 H_n^{(1,2)}(k_{p,0} r_2) e^{in\phi_2}. \tag{B5}$$

In the above equations, $\{A_n^1 \ldots A_n^4,\ B_n^1 \ldots B_n^4,\ C_n^1 \ldots C_n^4,\ D_n^1 \ldots D_n^4\}$ are the amplitudes of azimuthal harmonics, $k_{p,j}^2 = k_j^2 - k_z^2$, $k_j = k_0 \varepsilon_{r_j}$ $(j = 0 \ldots 4)$, $\varepsilon_{r_j} = \varepsilon_j/\varepsilon_0$ is the relative permittivity, $k_0^2 = \omega^2 \varepsilon_0 \mu_0$, $J_n(\cdot)$ and $Y_n(\cdot)$ are the Bessel function of the first and second kinds, respectively, and $H_n^{(1)}(\cdot)$ and $H_n^{(2)}(\cdot)$ are the Hankel functions of the first and second kinds, which take into account the damping of the wave field at infinity: $E_z^0 \to 0$ and $H_z^0 \to 0$ for $r_1, r_2 \to \infty$. The coordinates (r_1, ϕ_1) and (r_2, ϕ_2) in region 0 are related by the Graph addition theorem [59]

$$B_n(r_1) e^{\pm in\phi_1} = \sum_{k=-N}^{N} B_{n+k}(h) J_k(r_2) e^{\mp ik\phi_2} e^{\pm ik\pi},$$

$$B_n(r_2) e^{\pm in\phi_2} = \sum_{k=-N}^{N} B_{n+k}(h) J_k(r_1) e^{\mp ik\phi_1} e^{\pm in\pi}, \tag{B6}$$

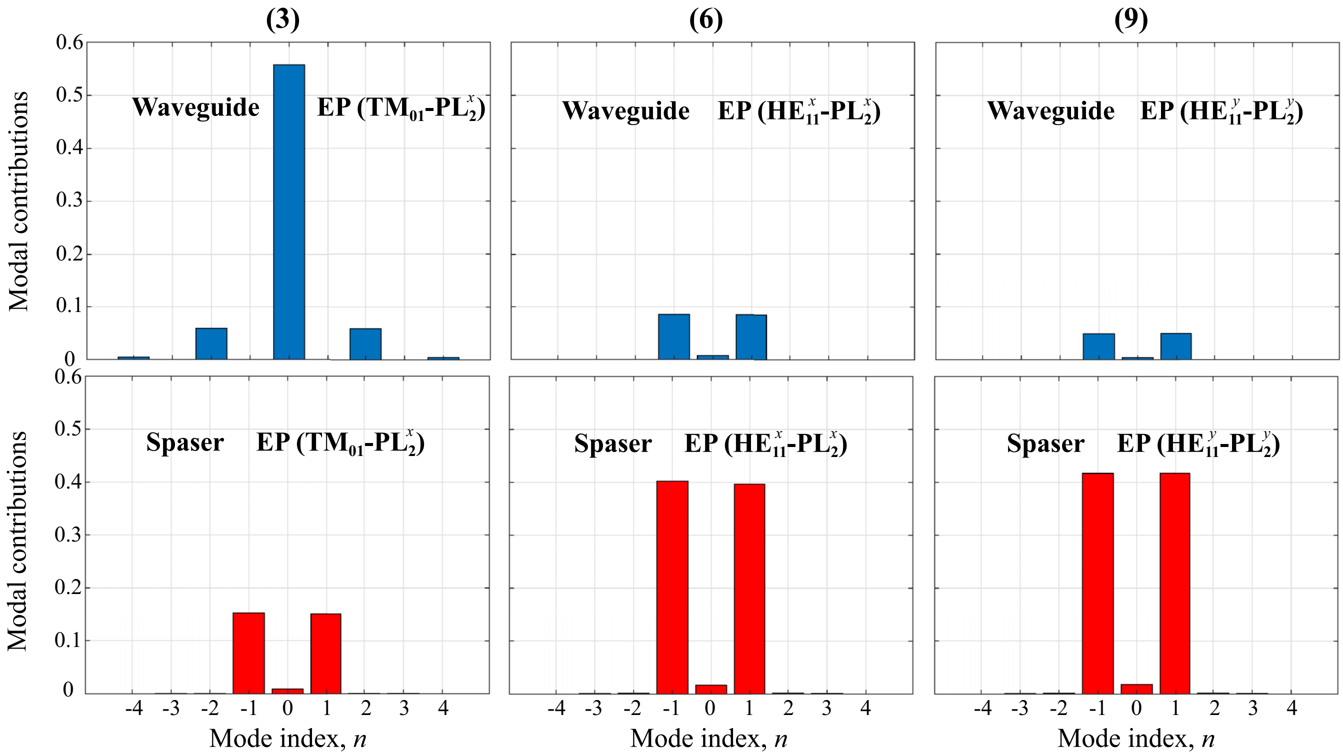

FIG. 6. Modal contributions to the electric energy of the system of the coupled waveguide (blue bars) and spaser (red bars) at the exceptional points (3), (6), and (9) depicted in Fig. 4.

where $B_n(\cdot)$ is the nth-order cylindrical function and h is the distance between the centers of the waveguide and spaser (see Fig. 1).

The azimuthal field components E_ϕ and H_ϕ are expressed in terms of E_z and H_z. The sought-for amplitudes $\{A_n^1 \dots A_n^4, B_n^1 \dots B_n^4, C_n^1 \dots C_n^4, D_n^1 \dots D_n^4\}$ and frequency ω are found from the continuity conditions for tangential field components at the interface surfaces

$$\begin{aligned}
\{E^1_{z,\phi}; H^1_{z,\phi}\}(R_1, \phi_1) &= \{E^0_{z,\phi}; H^0_{z,\phi}\}(R_1, \phi_1),\\
\{E^4_{z,\phi}; H^4_{z,\phi}\}(R_4, \phi_2) &= \{E^0_{z,\phi}; H^0_{z,\phi}\}(R_4, \phi_2),\\
\{E^2_{z,\phi}; H^2_{z,\phi}\}(R_2, \phi_2) &= \{E^3_{z,\phi}; H^3_{z,\phi}\}(R_2, \phi_2),\\
\{E^3_{z,\phi}; H^3_{z,\phi}\}(R_3, \phi_2) &= \{E^4_{z,\phi}; H^4_{z,\phi}\}(R_3, \phi_2). \qquad \text{(B7)}
\end{aligned}$$

The system of Eqs. (B7) has nontrivial solutions, once its determinant is zero. This condition yields the dispersion relation for eigenfrequencies of the coupled spaser-dielectric waveguide system immersed in free space.

APPENDIX C: GAUSSIAN BEAM

In the coordinate frame (η, ξ), the η-polarized Gaussian beam has the following form [60]:

$$\mathbf{E}_b(\eta, \xi) = \mathbf{E}_{b_0} \frac{w_0}{w(\eta)} e^{-\frac{(\xi-\xi_0)^2}{w^2(\eta)}} e^{-ik\eta} e^{-ik\frac{(\xi-\xi_0)^2}{2R(\eta)}} e^{i\phi(\eta)}, \qquad \text{(C1)}$$

where

$$w(\eta) = w_0\sqrt{1 + \frac{(\eta-\eta_0)^2}{p_0^2}},$$

$$R(\eta) = (\eta-\eta_0)\left(1 + \frac{p_0^2}{(\eta-\eta_0)^2}\right),$$

$$\phi(\eta) = \tan^{-1}\frac{\eta-\eta_0}{p_0},$$

$p_0 = \pi w_0^2/\lambda$, w_0 is the minimum width of the Gaussian beam, p_0 is the Rayleigh range, λ is the wavelength, and $\mathbf{E}_{b_0}$ is the electric field amplitude of the Gaussian beam, $w(\cdot)$ is the beam radius, $R(\cdot)$ is the radius of curvature of the wavefronts, and $\phi(\cdot)$ is the Gouy phase shift.

APPENDIX D: MODAL CONTRIBUTIONS

To study the contributions of the waveguide and spaser modes to the total electric energy stored in the system, we expand the electric field into the following series [61,62]:

$$\mathbf{E}(r, \phi) = \sum_{n=-N}^{N} \mathbf{A}_n(r) e^{in\phi},$$

$$\mathbf{A}_n(r) = \int_0^{2\pi} \mathbf{E}(r, \phi) e^{-in\phi} d\phi, \qquad \text{(D1)}$$

where r and ϕ are coordinates of the chosen cylindrical coordinate frame and $\mathbf{A}_n(r)$ are the expansion coefficients.

Substitution of coefficients (D1) into the electric energy equation (1) yields

$$U_e = \frac{1}{2}\int_0^{2\pi}\int_0^R \varepsilon(r,\phi)[\mathbf{E}(r,\phi)\cdot\mathbf{E}^*(r,\phi)]r dr d\phi$$
$$= \pi\sum_{n=-N}^{N}\int_0^R \varepsilon(r)||\mathbf{A}_n(r)||^2 r dr = \sum_{n=-N}^{N} U_e^n, \quad (D2)$$
$$U_e^n = \pi\int_0^R \varepsilon(r)||\mathbf{A}_n(r)||^2 r dr. \quad (D3)$$

Here R is the radius of the cylinder system under consideration (in our case, for the waveguide $0 \leqslant r \leqslant R_1$ and for the spaser $0 \leqslant r \leqslant R_4$). The obtained values of U_e^n make it possible to find the electric energy of each mode. Then the modal contributions can be derived from the relation U_e^n/U_e.

In Fig. 6, the contributions of separate modes to the total electric energy are collected. They are calculated for the system parameters at the corresponding exceptional points shown in Fig. 4. Since this work considers a coupled system, the contributions of modes to the electric energy of the waveguide (photonic subsystem) and spaser (plasmonic subsystem) are presented separately.

[1] J. B. Pendry, A. Aubry, D. R. Smith, and S. A. Maier, Transformation optics and subwavelength control of light, Science **337**, 549 (2012).
[2] A. F. Koenderink, A. Alù, and A. Polman, Nanophotonics: Shrinking light-based technology, Science **348**, 516 (2015).
[3] A. Krasnok and A. Alù, Active nanophotonics, Proc. IEEE **108**, 628 (2020).
[4] C. E. Rüter, K. G. Makris, R. El-Ganainy, D. N. Christodoulides, M. Segev, and D. Kip, Observation of parity-time symmetry in optics, Nat. Phys. **6**, 192 (2010).
[5] O. V. Shramkova and G. P. Tsironis, Propagation of electromagnetic waves in PT-symmetric hyperbolic structures, Phys. Rev. B **94**, 035141 (2016).
[6] L. Feng, R. El-Ganainy, and L. Ge, Non-Hermitian photonics based on parity–time symmetry, Nat. Photon. **11**, 752 (2017).
[7] Ş. K. Özdemir, S. Rotter, F. Nori, and L. Yang, Parity-time symmetry and exceptional points in photonics, Nat. Mater. **18**, 783 (2019).
[8] M.-A. Miri and A. Alù, Exceptional points in optics and photonics, Science **363**, eaar7709 (2019).
[9] P. Berini and I. De Leon, Surface plasmon-polariton amplifiers and lasers, Nat. Photonics **6**, 16 (2012).
[10] N. M. Estakhri and A. Alù, Physics of unbounded, broadband absorption/gain efficiency in plasmonic nanoparticles, Phys. Rev. B **87**, 205418 (2013).
[11] S. I. Azzam, A. V. Kildishev, R.-M. Ma, C.-Z. Ning, R. Oulton, V. M. Shalaev, M. I. Stockman, J.-L. Xu, and X. Zhang, Ten years of spasers and plasmonic nanolasers, Light Sci. Appl. **9**, 90 (2020).
[12] S. Xiao, V. P. Drachev, A. V. Kildishev, X. Ni, U. K. Chettiar, H.-K. Yuan, and V. M. Shalaev, Loss-free and active optical negative-index metamaterials, Nature (London) **466**, 735 (2010).
[13] J. Yu, B. Ma, A. Ouyang, P. Ghosh, H. Luo, A. Pattanayak, S. Kaur, M. Qiu, P. Belov, and Q. Li, Dielectric super-absorbing metasurfaces via PT symmetry breaking, Optica **8**, 1290 (2021).
[14] A. V. Hlushchenko, D. V. Novitsky, and V. R. Tuz, Trapped-mode excitation in all-dielectric metamaterials with loss and gain, Phys. Rev. B **106**, 155429 (2022).
[15] S. Bittner, B. Dietz, U. Günther, H. L. Harney, M. Miski-Oglu, A. Richter, and F. Schäfer, PT symmetry and spontaneous symmetry breaking in a microwave billiard, Phys. Rev. Lett. **108**, 024101 (2012).
[16] J. Schindler, A. Li, M. C. Zheng, F. M. Ellis, and T. Kottos, Experimental study of active LRC circuits with $\mathcal{PT}$ symmetries, Phys. Rev. A **84**, 040101(R) (2011).
[17] H. Jing, S. K. Özdemir, X.-Y. Lü, J. Zhang, L. Yang, and F. Nori, PT-symmetric phonon laser, Phys. Rev. Lett. **113**, 053604 (2014).
[18] X. Zhu, H. Ramezani, C. Shi, J. Zhu, and X. Zhang, PT-symmetric acoustics, Phys. Rev. X **4**, 031042 (2014).
[19] W.-J. Yang, Z.-Z. Yang, A.-Y. Guan, X.-Y. Zou, and J.-C. Cheng, Design and experimental demonstration of effective acoustic gain medium for PT-symmetric refractive index, Appl. Phys. Lett. **120**, 063503 (2022).
[20] E. Snitzer, Cylindrical dielectric waveguide modes, J. Opt. Soc. Am. **51**, 491 (1961).
[21] R. K. Mongia and P. Bhartia, Dielectric resonator antennas – a review and general design relations for resonant frequency and bandwidth, Int. J. Microwave Wireless Technol. **4**, 230 (1994).
[22] D. B. Keck and R. D. Maurer, Optical pulse broadening in long fibre waveguides, Opt. Laser Technol. **7**, 229 (1975).
[23] S. Ramachandran, P. Kristensen, and M. F. Yan, Generation and propagation of radially polarized beams in optical fibers, Opt. Lett. **34**, 2525 (2009).
[24] *Fundamentals of Optical Fibre Communications*, 2nd ed., edited by M. K. Bamoski (Academic Press, New York, 1981).
[25] M. Koshiba, K. Hayata, and M. Suzuki, Finite-element solution of anisotropic waveguides with arbitrary tensor permittivity, J. Lightwave Technol. **4**, 121 (1986).
[26] S. Ramachandran, S. Golowich, M. F. Yan, E. Monberg, F. V. Dimarcello, J. Fleming, S. Ghalmi, and P. Wisk, Lifting polarization degeneracy of modes by fiber design: A platform for polarization-insensitive microbend fiber gratings, Opt. Lett. **30**, 2864 (2005).
[27] J. Zhao, M. Tang, K. Oh, Z. Feng, C. Zhao, R. Liao, S. Fu, P. P. Shum, and D. Liu, Polarization-maintaining few mode fiber composed of a central circular-hole and an elliptical-ring core, Photon. Res. **5**, 261 (2017).
[28] S. Chen and J. Wang, Fully degeneracy-lifted bow-tie elliptical ring-core multi-mode fiber, Opt. Express **26**, 18773 (2018).
[29] D. V. Novitsky, CPA-laser effect and exceptional points in PT-symmetric multilayer structures, J. Opt. **21**, 085101 (2019).

[30] T. Fujisawa and K. Saitoh, Arbitrary higher-order optical spatial state generation by using spontaneously broken degeneracy modes in helically twisted ring-core hole assisted fibers, Opt. Express **30**, 24565 (2022).
[31] A. S. Kupriianov, V. I. Fesenko, A. B. Evlyukhin, W. Han, and V. R. Tuz, Trapped mode control in metasurfaces composed of particles with the form birefringence property, Opt. Express **31**, 6996 (2023).
[32] S. I. Lepeshov, A. E. Krasnok, P. A. Belov, and A. E. Miroshnichenko, Hybrid nanophotonics, Phys. Usp. **61**, 1035 (2019).
[33] Á. Barreda, F. Vitale, A. E. Minovich, C. Ronning, and I. Staude, Applications of hybrid metal-dielectric nanostructures: State of the art, Adv. Photon. Res. **3**, 2100286 (2022).
[34] F. Tang, P.-M. Adam, and S. Boutami, Theoretical investigation of SERS nanosensors based on hybrid waveguides made of metallic slots and dielectric strips, Opt. Express **24**, 21244 (2016).
[35] Y. Sun, I. Sinev, A. Zalogina, E. Ageev, H. Shamkhi, F. Komissarenko, I. Morozov, S. Lepeshov, V. Milichko, S. Makarov, I. Mukhin, and D. Zuev, Reconfigurable near-field enhancement with hybrid metal-dielectric oligomers, Laser Photon. Rev. **13**, 1800274 (2019).
[36] S. Sarkar, V. Gupta, M. Kumar, J. Schubert, P. T. Probst, J. Joseph, and T. A. F. Köunig, Hybridized guided-mode resonances via colloidal plasmonic self-assembled grating, ACS Appl. Mater. Interfaces **11**, 13752 (2019).
[37] A. Maimaiti, P. P. Patra, S. Jones, T. J. Antosiewicz, and R. Verre, Low-loss hybrid high-index dielectric particles on a mirror for extreme light confinement, Adv. Opt. Mater. **8**, 1901820 (2020).
[38] V. A. Milichko, D. A. Zuev, D. G. Baranov, G. P. Zograf, K. Volodina, A. A. Krasilin, I. S. Mukhin, P. A. Dmitriev, V. V. Vinogradov, S. V. Makarov *et al.*, Metal-dielectric nanocavity for real-time tracing molecular events with temperature feedback, Laser Photon. Rev. **12**, 1700227 (2018).
[39] H. J. Kim, J. Jun, H.-J. Choi, H. Kwon, J. Park, C. Seo, J. K. Kim, J. Shin, J. Kim, H. Lee *et al.*, Pyramidal metal–dielectric hybrid-structure geometry with an asymmetric TiO_2 layer for broadband light absorption and photocatalytic applications, Nano Energy **53**, 468 (2018).
[40] C. Han, S.-H. Li, Z.-R. Tang, and Y.-J. Xu, Tunable plasmonic core-shell heterostructure design for broadband light driven catalysis, Chem. Sci. **9**, 8914 (2018).
[41] S. Sun, M. Li, Q. Du, C. E. Png, and P. Bai, Metal-dielectric hybrid dimer nanoantenna: Coupling between surface plasmons and dielectric resonances for fluorescence enhancement, J. Phys. Chem. C **121**, 12871 (2017).
[42] S. Sun, T. Zhang, Q. Liu, L. Ma, Q. Du, and H. Duan, Enhanced directional fluorescence emission of randomly oriented emitters via a metal-dielectric hybrid nanoantenna, J. Phys. Chem. C **123**, 21150 (2019).
[43] D. V. Novitsky, V. R. Tuz, S. L. Prosvirnin, A. V. Lavrinenko, and A. V. Novitsky, Transmission enhancement in loss-gain multilayers by resonant suppression of reflection, Phys. Rev. B **96**, 235129 (2017).
[44] R. Miao, Y. Hu, H. Ouyang, Y. Tang, C. Zhang, J. You, X. Zheng, Z. Xu, T. Jiang *et al.*, A polarized nonlinear optical response in a topological insulator Bi_2Se_3-Au nanoantenna hybrid-structure for all-optical switching, Nanoscale **11**, 14598 (2019).
[45] S. Busschaert, N. Flöry, S. Papadopoulos, M. Parzefall, S. Heeg, and L. Novotny, Beam steering with a nonlinear optical phased array antenna, Nano Lett. **19**, 6097 (2019).
[46] D. J. Bergman and M. I. Stockman, Surface plasmon amplification by stimulated emission of radiation: Quantum generation of coherent surface plasmons in nanosystems, Phys. Rev. Lett. **90**, 027402 (2003).
[47] M. I. Stockman, Spasers explained, Nat. Photon. **2**, 327 (2008).
[48] M. A. Noginov, G. Zhu, A. M. Belgrave, R. Bakker, V. M. Shalaev, E. E. Narimanov, S. Stout, E. Herz, T. Suteewong, and U. Wiesner, Demonstration of a spaser-based nanolaser, Nature (London) **460**, 1110 (2009).
[49] R. F. Oulton, V. J. Sorger, T. Zentgraf, R.-M. Ma, C. Gladden, L. Dai, G. Bartal, and X. Zhang, Plasmon lasers at deep subwavelength scale, Nature (London) **461**, 629 (2009).
[50] A. A. E. Saleh and J. A. Dionne, Waveguides with a silver lining: Low threshold gain and giant modal gain in active cylindrical and coaxial plasmonic devices, Phys. Rev. B **85**, 045407 (2012).
[51] H. Ow, D. R. Larson, M. Srivastava, B. A. Baird, W. W. Webb, and U. Wiesner, Bright and stable core-shell fluorescent silica nanoparticles, Nano Lett. **5**, 113 (2005).
[52] H. Gogoi, S. Banerjee, and A. Datta, Photoluminescent silica nanostructures and nanohybrids, ChemPhysChem **23**, e202200280 (2022).
[53] T. P. White, B. T. Kuhlmey, R. C. McPhedran, D. Maystre, G. Renversez, C. M. de Sterke, and L. C. Botten, Multipole method for microstructured optical fibers. I. Formulation, J. Opt. Soc. Am. B **19**, 2322 (2002).
[54] A. V. Hlushchenko, V. I. Shcherbinin, D. V. Novitsky, and V. R. Tuz, Multimode parity-time symmetry and loss compensation in coupled waveguides with loss and gain, Phys. Rev. A **104**, 013507 (2021).
[55] *Handbook of Optical Constants of Solids*, edited by E. D. Palik, (Academic Press, San Diego, CA, 1998).
[56] W. D. Heiss, The physics of exceptional points, J. Phys. A: Math. Theor. **45**, 444016 (2012).
[57] G. Vallone, On the properties of circular beams: Normalization, Laguerre–Gauss expansion, and free-space divergence, Opt. Lett. **40**, 1717 (2015).
[58] S. Kim, D. A. Westly, B. J. Roxworthy, Q. Li, A. Yulaev, K. Srinivasan, and V. A. Aksyuk, Photonic waveguide to free-space Gaussian beam extreme mode converter, Light Sci. Appl. **7**, 72 (2018).
[59] *Handbook of Mathematical Functions with Formulas, Graphs, and Mathematical Tables*, edited by M. Abramowitz and I. A. Stegun, Applied Mathematics Series, Vol. 55 (National Bureau of Standards, Washington, DC, 1965), Chap. 9.
[60] O. Svelto, *Principles of Lasers*, 5th ed. (Springer, New York, 2016).
[61] O. Shapira, A. F. Abouraddy, J. D. Joannopoulos, and Y. Fink, Complete modal decomposition for optical waveguides, Phys. Rev. Lett. **94**, 143902 (2005).
[62] J. Pinnell, I. Nape, B. Sephton, M. A. Cox, V. Rodríguez-Fajardo, and A. Forbes, Modal analysis of structured light with spatial light modulators: A practical tutorial, J. Opt. Soc. Am. A **37**, C146 (2020).